Geochemistry Geophysics Geosystems G3
AN ELECTRONIC JOURNAL OF THE EARTH SCIENCES
Published by AGU and the Geochemical Society

Article
Volume 4, Number 9
19 September 2003
1070, doi:10.1029/2002GC000446
ISSN: 1525-2027

Geodetic determination of relative plate motion and crustal deformation across the Scotia-South America plate boundary in eastern Tierra del Fuego

R. Smalley, Jr.
Center for Earthquake Research and Information, University of Memphis, 3876 Central Avenue, Ste. 1, Memphis, Tennessee 38152, USA (rsmalley@memphis.edu)

E. Kendrick and M. G. Bevis
School of Ocean, Earth and Space Technology, University of Hawaii, 1680 East West Road, Honolulu, Hawaii 96822, USA (kendrick@soest.hawaii.edu; bevis@hawaii.edu)

I. W. D. Dalziel and F. Taylor
Institute of Geophysics, Jackson School of Geosciences, University of Texas at Austin, 4412 Spicewood Springs Road, Building 600, Austin, Texas 78759, USA (ian@utig.ig.utexas.edu; fred@utig.ig.utesas.edu)

E. Lauría
Instituto Geográfico Militar de Argentina, Cabildo 381, 1426 Buenos Aires, Argentina (jdivgeod@mapas.igm.gov.ar)

R. Barriga
Instituto Geográfico Militar de Chile, Nueva Santa Isabel 1640, Santiago, Chile (rbarriga@igm.cl)

G. Casassa
Centro de Estudios Científicos, Avda. Arturo Prat 514, Casilla 1469, Valdivia, Chile (gcasassa@cecs.cl)

E. Olivero and E. Piana
Centro Austral de Investigaciones Científicas, Av. Malvinas Argentinas s/n, Caja de Correo 92, 9410 Ushuaia, Tierra del Fuego, Argentina (emolivero@ciudad.com.ar; arqueologia@tierradelfuego.org.ar)

[1] Global Positioning System (GPS) measurements provide the first direct measurement of plate motion and crustal deformation across the Scotia-South America transform plate boundary in Tierra del Fuego. This plate boundary accommodates a part of the overall motion between South America and Antarctica. The subaerial section of the plate boundary in Tierra del Fuego, about 160 km in length, is modeled as a two dimensional, strike-slip plate boundary with east-west strike. Along the Magallanes-Fagnano fault system, the principal fault of this portion of the plate boundary, relative plate motion is left-lateral strike-slip on a vertical fault at 6.6 ± 1.3 mm/year based on an assumed locking depth of 15 km. The site velocities on the Scotia Plate side are faster than the relative velocity by an additional 1–2 mm/yr, suggesting there may be a wider region of diffuse left-lateral deformation in southern Patagonia. The north-south components of the velocities, however, do not support the existence of active, large-scale transpression or transtension between the South America and Scotia plates along this section of the plate boundary.

Components: 9235 words, 7 figures, 2 tables.

Keywords: Crustal deformation; plate movement; South America; Scotia Arc.

Index Terms: 1206 Geodesy and Gravity: Crustal movements—interplate (8155); 1243 Geodesy and Gravity: Space geodetic surveys.

Received 23 September 2002; **Revised** 15 April 2003; **Accepted** 15 May 2003; **Published** 19 September 2003.

Smalley, R., Jr., E. Kendrick, M. G. Bevis, I. W. D. Dalziel, F. Taylor, E. Lauría, R. Barriga, G. Casassa, E. Olivero, and E. Piana, Geodetic determination of relative plate motion and crustal deformation across the Scotia-South America plate boundary in eastern Tierra del Fuego, *Geochem. Geophys. Geosyst.*, *4*(9), 1070, doi:10.1029/2002GC000446, 2003.

1. Introduction

[2] The Scotia Arc Project (Figure 1) is using GPS geodesy to study the geodynamics of the Scotia Arc and surrounding regions. The Scotia Arc is composed of the Scotia and South Sandwich Plates, which are small, young, and principally oceanic plates. These plates formed in response to changes in the relative plate motions of South America and Antarctica during the past 30 Myr [*Barker et al.*, 1991]. The Scotia-South America plate boundary is a mostly submarine transform boundary defined by the North Scotia Ridge [*British Antarctica Survey*, 1985]. It is the northernmost of three, left-lateral transform faults defining the north, west, and south sides of the Scotia plate. Relative motion between South America and Antarctica appears to be partitioned between these three fault systems, although the relative partitioning between the faults is poorly known.

[3] The western end of the North Scotia Ridge continues along-strike, traversing the island of Tierra del Fuego as the Magallanes-Fagnano fault system (Figure 1, Figures 2a and 2b). Geological evidence indicates this is the active plate boundary, or at least the most active component [*Olivero et al.*, 1995; *Olivero and Malumián*, 1999; *Schwartz et al.*, 2001; *Olivero and Martinioni*, 2001; *Lodolo et al.*, 2002]. Several major sub-parallel faults, including a fault along the Lasifashaj Valley, an inferred fault in the Beagle Channel and a fault through Lago Deseado, could also accommodate part of the plate motion (Figure 2b). Continuing to the west, the Magallanes-Faganano fault returns to a subaqueous setting in Lago Fagnano, Seno Almirantazgo and the Straits of Magellan as it bends to a more northwesterly strike becoming one limb of a complex, diffuse, unstable trench-trench-transform triple junction between the Antarctic, South America and Scotia plates [*Forsythe*, 1975; *Cunningham*, 1993].

[4] The North Scotia Ridge has a long wavelength, 1,000 km scale, S-shape (Figure 1). Sidescan sonar studies along the North Scotia Ridge south of the Falkland/Malvinas Islands indicate plate motion in that region is currently pure strike-slip [*Cunningham et al.*, 1998]. Recent marine seismic studies east of Tierra del Fuego, along the oceanward extension of the Magallanes-Fagnano fault, image an asymmetric basin. This basin is interpreted to be a transtensional pull-apart structure, formed between the main plate boundary fault on the north and a complex set of small normal faults on the south [*Lodolo et al.*, 2002]. To the west of Lago Fagnano, the plate boundary turns northwest through Seno Almirantazgo and the Straits of Magellan in a restraining bend geometry, although geological studies have proposed both transtensional and transpressional interpretations for development of the structures in this region [*Cunningham*, 1993].

[5] Before the breakup of Gondwana, the Andes are thought to have been continuous from South America to the Antarctic Peninsula [*Dalziel and Elliot*, 1971; *DeWit*, 1977; *Dalziel*, 1989; *Cunningham et al.*, 1995]. As a consequence of the relative South America-Antarctica plate motion and coeval formation of the Scotia plate, the north-south striking southernmost Andes were sheared and rotated 90° counterclockwise, becoming part of the Scotia-South America plate boundary [*Cunningham et al.*, 1991; *Cunningham*, 1993; *Kraemer*, 1999; *Diraison et al.*, 2000]. This process probably continues today, as there are young rift structures north of the strike-slip plate boundary (Figures 2a and 2b)

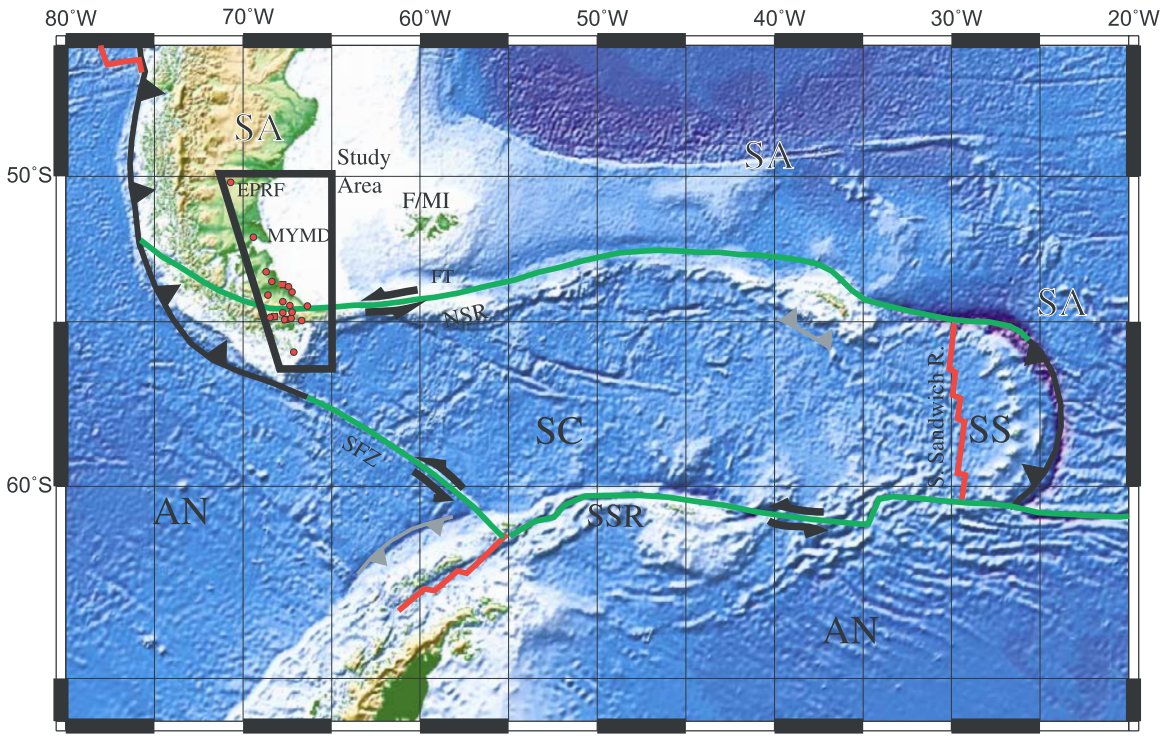

Figure 1. Tectonic map of Scotia Arc and GPS network. Red squares, continuous GPS stations, red circles, campaign GPS sites. Study area shown by black outline. Mapped plate boundaries modified from PLATES project [*Coffin et al.*, 1998]. Plate boundaries: subduction (black), ridges (red), and transforms (green). SA, South America plate; AN, Antarctic plate; SC, Scotia plate; SS, South Sandwich plate; NSR, North Scotia Ridge; SSR, South Scotia Ridge; SFZ, Shackleton Fracture Zone; AP, Antarctic Peninsula; DP, Drake Passage; F/MI, Falkland/Malvinas Islands. All the major transforms bordering the Scotia Plate (NSR, SSR, SFZ) are left-lateral.

[*Diraison et al.*, 1997, 2000]. This suggests a model similar to western North America where deformation is partitioned between a well-defined plate boundary along the San Andreas transform fault plus a wider area of distributed deformation in the Basin and Range [*Atwater*, 1970]. The rift structures of Tierra del Fuego and southern Patagonia are also consistent with tectonics due to drag around the southwest corner of South America [*Diraison et al.*, 1997, 2000], suggesting a continuing development of the Patagonian orocline. As a consequence of the oroclinal bending, the strikes of lithologic boundaries and older structures produced by previous episodes of compressional plate boundary tectonics are now parallel to the strike of the active transform plate boundary. Many of these older faults have been reactivated as strike-slip faults [*Winslow*, 1981], but estimation of strike-slip displacement and displacement rate has been hindered by the lack of piercing points due to the changes in lithology across the faults. *Olivero et al.* [1995] estimated that a minimum of 30 km of displacement has occurred during the past 30 Myr.

[6] Finally, before and during the last glacial maximum, glaciers carved out many of the presumably weak fault zones leaving long deep valleys. Lago Fagnano, Seno Almirantazgo, the Beagle Channel, the Straits of Magellan, the San Sabastián and Inútil Bays, and the rift structures in northern Tierra del Fuego occupy such valleys (Figures 2a and 2b). Many of these valleys are now drowned fiords, lakes or bays. This makes it difficult to determine if they contain active faults, if the faults are locked or creeping, the amount of offset, and the relative contribution to their formation of transpressional pull-apart tectonics versus glacial carving. Where the trace of the faults outcrop subaerially, along with much of the lower elevation and low relief areas of Tierra del Fuego, the surface is covered with either very young glacial

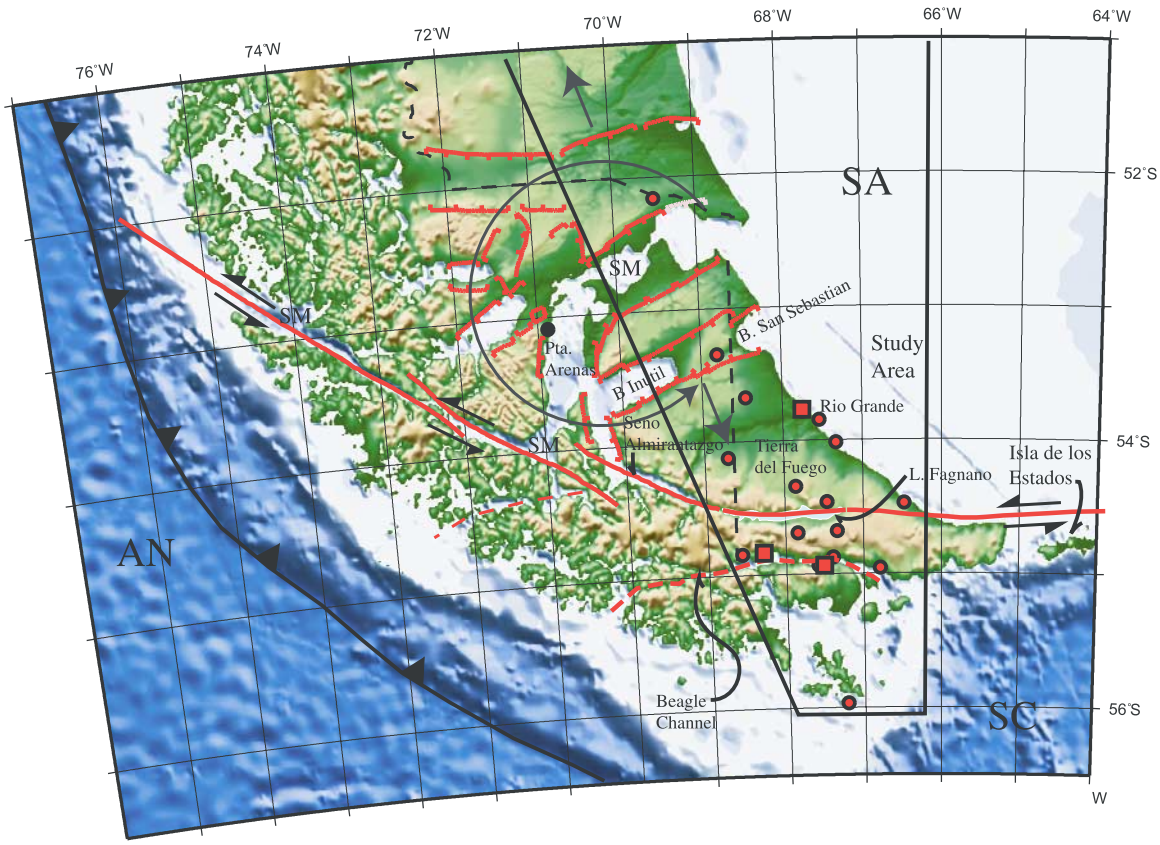

Figure 2a. Map of the Scotia-South America-Antarctica triple junction region, study area and GPS network. Symbols are as in Figure 1, except strike-slip boundary, modified from *Cunningham* [1993], *Klepeis* [1994] and *Diraison et al.* [1997], through Tierra del Fuego, in red. Dashed red lines for inferred faults. Active normal faulting north of 54°S is after *Diraison et al.* [1997] (ticks on downthrown sides). The NNW-SSE oriented gray arrows show proposed extensional tectonics north of main plate boundary and the gray circular arrow shows proposed block rotation around the triple junction corner of South America after *Diraison et al.* [1997]. Antarctic-South America subduction boundary is shown by black line. SM: Straits of Magellan.

deposits or peat. This further limits geologically addressing the questions above. To date, geomorphologic evidence of active deformation associated with earthquakes along the fault has been observed [*Olivero et al.*, 1995; *Olivero and Malumián*, 1999; *Schwartz et al.*, 2001; *Olivero and Martinioni*, 2001; *Lodolo et al.*, 2002] but no evidence has been reported for fault creep.

[7] There is a very low level of seismicity observed along the South America-Scotia boundary [*Pelayo and Wiens*, 1989; *Adarnos et al.*, 1999]. Some local seismicity has been recorded, however, that suggests microseismic activity generally follows the Fagnano-Magallanes fault [*Febrer et al.*, 2000]. A small cluster of events was also found in the Beagle Channel [*Febrer et al.*, 2000]. The low level of seismicity along the plate boundary as a whole is generally thought to be due to the slow rate of movement between the two plates across a locked fault [*Pelayo and Wiens*, 1989; *Adarnos et al.*, 1999; *Lodolo et al.*, 2002]. Locally, especially along the westernmost section of the plate boundary in Tierra del Fuego, aseismic creep may also be a factor. Distinguishing between these two cases is important in the estimation of seismic hazard [*Bürgmann et al.*, 1998]. The plate boundary passes between the two principal cities of Argentine Tierra del Fuego. Rio Grande (location of site RIOG, Figure 3), a manufacturing and oil production center, is about 75 km to the north; Ushuaia (location of site AUTF, Figure 3), a manufacturing center and port, is about 35 km to the south. An

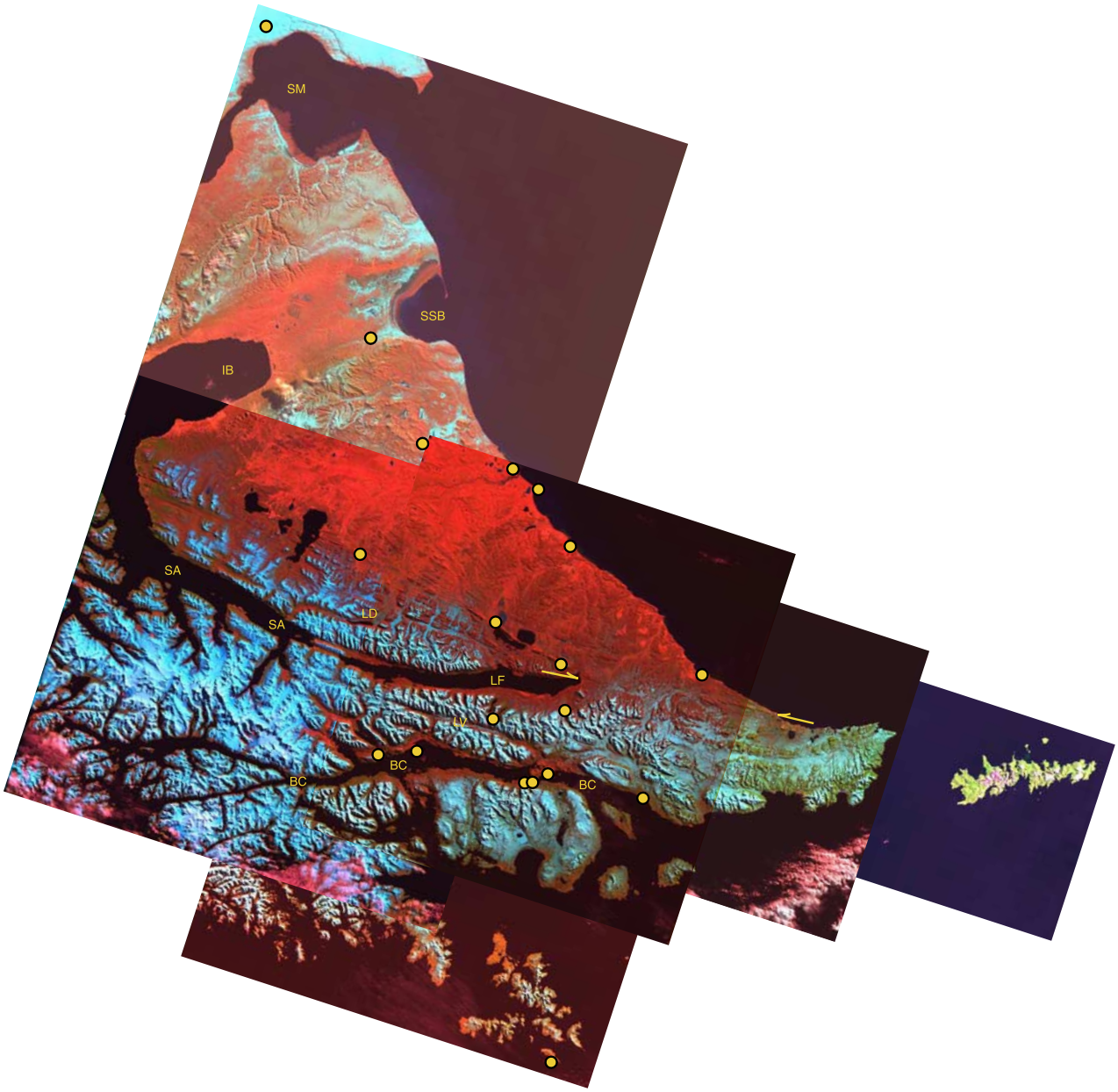

Figure 2b. Mosaic of LANDSAT-TM browse images. SM, Straits of Magellan; SA, Seno Almirantazgo; SSB, San Sebastián Bay; IB, Inútil Bay; LF, Lago Fagnano; LD, Lago Deseado; LV, Lasifashaj Valley; BC, Beagle Channel; arrows indicate ends of lineament, which is surface expression of Magallanes-Fagnano fault. Yellow filled circles show locations of GPS sites.

important gas pipeline and the only road to Ushuaia cross the plate boundary near the eastern end of Lago Fagnano. The plate boundary is also near the Chilean port city of Punta Arenas (Figure 2a) located on the Straits of Magellan. Each of these cities has a population of about 50,000.

[8] The earliest report of seismic activity in Tierra del Fuego was associated with an earthquake in 1879 [*Bridges*, 1879]. The event was widely felt and walking was difficult in Ushuaia where it woke most people [*Bridges*, 1879]. *Lomnitz* [1970] estimated this event had a magnitude of 7. In 1949 a pair of

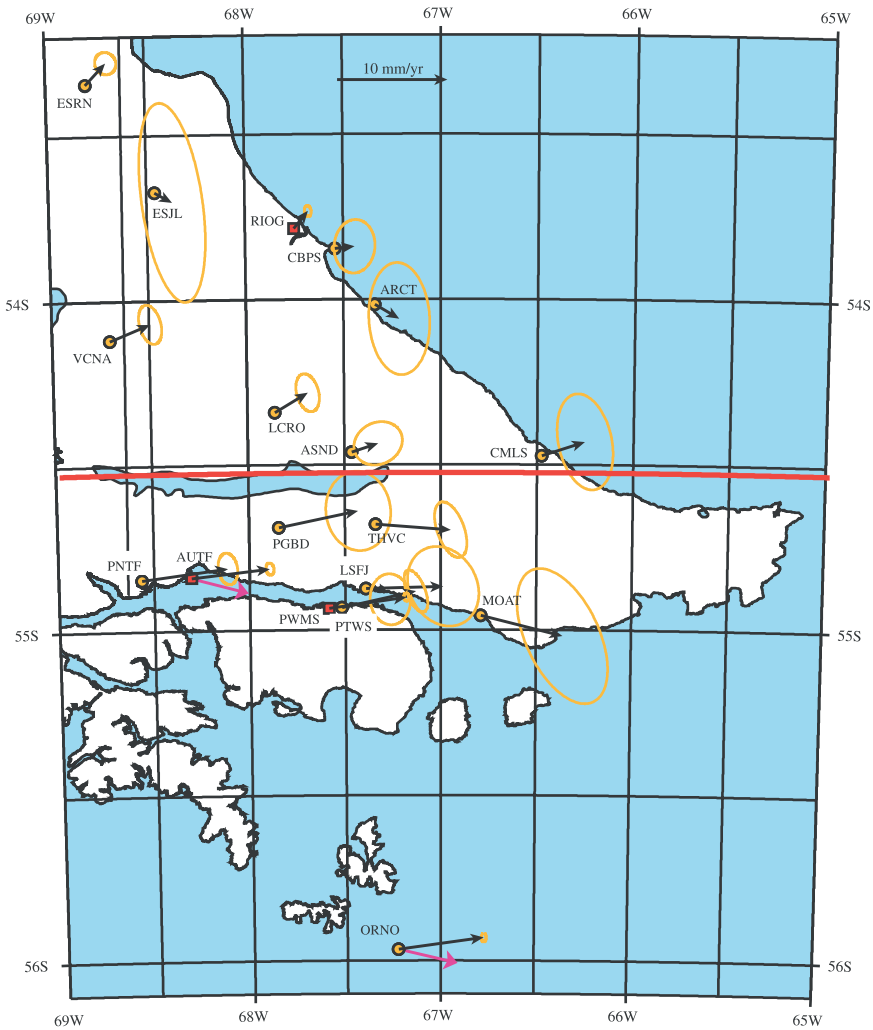

Figure 3. GPS velocities with respect to stable South America. The 95% error ellipses are shown for the sites (orange filled circles) used to invert for fault parameters. Symbols, plate boundaries and other faults are as in Figures 1 and 2. Best-fit location for E-W striking, vertical, two-dimensional strike-slip fault indicated by red line subparallel to Magallanes-Fagnano fault. Purple vectors show velocities predicted by the Scotia-South America Euler Pole of *Pelayo and Wiens* [1989] for two sites.

large earthquakes, felt strongly throughout Patagonia, struck Tierra del Fuego about 9 hours apart. *Pelayo and Wiens* [1989] report a magnitude of 7.75 for the first event, but none for the second, while *Jaschek et al.* [1982] report a magnitude of 7.5 for the second, but none for the first. The ISC catalog does not report magnitudes for either event, but the second event produced larger intensities in Punta Arenas, suggesting it was either larger and/or closer to Punta Arenas than the first. The PDE and ISC locations, and relocations by *Pelayo and Wiens* [1989], are well off the Magallanes-Fagnano fault, although Pelayo and Weins' error ellipses include the fault. On the basis of surface rupture (one meter, vertical, north side up) that cut a road at the eastern end of Lago Fagnano (A. Goodall, personal communication) the first event occurred on the Magallanes-Fagnano fault. Goodall also reported liquifaction in the floodplain of the Rio Grande, near the city of Rio Grande, associated with the first event but did not report any with respect to the second. Liquifaction was also observed 150 km southwest of Punta Arenas [*Lomnitz*, 1970], although it is not known if it was caused by the first or second event. Horizontal offsets of fences of up to 5 meters were reported by the manager of a farm along the Atlantic coast where the Magallanes-Fagnano fault goes out to sea (E. Oyarzun, personal

Table 1. GPS Velocity Estimates With Respect to Stable South America[a]

Name	lat	lon	ve	se	vn	sn	ne corr	span	#meas
ARCT	−54.02	−67.34	2.20	1.47	−1.30	2.70	−0.06	2.04	3
ASND	−54.46	−67.46	2.40	1.05	0.80	0.94	0.15	2.98	4
AUTF	−54.84	−68.30	7.10	0.06	0.80	0.10	−0.14	4.65	cont
CBPS	−53.85	−67.54	1.80	0.88	0.20	1.15	0.06	2.97	4
CMLS	−54.47	−66.47	3.90	1.21	1.30	2.07	−0.26	2.95	4
EPRF	−50.23	−70.79	0.80	1.76	1.20	1.27	0.25	2.81	3
ESJL	−53.67	−68.46	1.60	1.56	−0.90	4.79	−0.34	2.05	3
ESRN	−53.34	−68.80	1.90	0.40	2.00	0.42	−0.06	5.66	2[d]
LCRO	−54.34	−67.86	3.00	0.51	1.80	0.82	−0.27	2.94	4
LSFJ	−54.87	−67.39	7.00	1.71	0.20	1.91	−0.17	2.07	3
MOAT	−54.96	−66.79	7.40	2.17	−1.80	3.23	−0.49	2.07	3
MYMD	−52.16	−69.50	1.10	0.26	1.20	0.43	−0.44	5.66	2[d]
ORNO	−55.97	−67.23	7.70	0.09	1.10	0.16	0.01	5.87	2[d]
PGBD	−54.69	−67.84	7.20	1.40	1.50	1.71	−0.04	2.97	4
PNTF	−54.84	−68.56	7.80	0.39	1.00	0.62	−0.14	4.04	4[b]
PTWS	−54.93	−67.52	6.70	0.44	1.50	0.78	−0.56	5.63	2[d]
PWMS	−54.93	−67.58	7.00	0.04	1.00	0.06	−0.15	5.10	cont
RIOG	−53.79	−67.75	1.30	0.05	1.60	0.08	−0.17	7.69	cont[c]
THVC	−54.68	−67.34	6.80	0.70	−0.50	1.20	−0.48	2.95	4
VCNA	−54.12	−68.70	3.70	0.43	1.50	0.73	−0.30	5.67	2[d]

[a] Columns list the site names, positions, velocities and their standard errors in mm/yr, the correlation between the north and east components (which specifies the azimuth of the error ellipse), the time span between first and last measurements, and the total number of measurements. Cont, continuous.
[b] Continuous for one year, then campaign measurements using the continuous station antenna mast and mount.
[c] Antenna monument not installed in rock.
[d] Tripod, non-choke ring antenna used during first measurement in 1994.

communication) and also by a member of a search and rescue team that followed the fault trace from Lago Fagnano east to the coast in 1950 (R. Sutherland, personal communication). Sutherland reported additional geomorphic features that, while not observed until a year after the earthquake sequence, are thought to be associated with the first event. Trenching on the still visible rupture trace of the 1949 event along the Magallanes-Fagnano fault indicates it has ruptured several times, although missing geologic section and lack of offset information precluded determination of average repeat times and magnitudes [*Schwartz et al.*, 2001]. There are no reports of surface rupture associated with the second event.

[9] This paper presents the results from a network of 20 GPS stations in Tierra del Fuego and southern Patagonia that spans the central portion of the Magallanes-Fagnano fault of the Scotia-South America transform boundary (Table 1, Figures 2 and 3). Although the time period sampled is short and the density of measurement points is low, GPS measurements can directly address the questions of plate movement and its partitioning among candidate faults, overcoming some of the geologic problems discussed above. The GPS measurements provide the first direct constraints on the rate of plate movement and associated crustal deformation along the westernmost portion of the Scotia-South America plate boundary.

2. Data Analysis

[10] In the austral summer of 1993–94 a sparse GPS network was installed and measured in Chilean Patagonia and Tierra del Fuego. Measurements were performed in a traditional GPS campaign. Between 1995 and 1997 a network of continuous GPS stations was installed throughout Argentina and Chile to support future fieldwork using the measurement strategy advocated by *Bevis et al.* [1997]. In this scheme, sites are measured individually, or in small groups, with respect to the continuous network. In 1998, in Argentina, the network was densified in Tierra del Fuego and expanded in southern Patagonia. As discussed earlier, many of the accessible areas of Tierra del Fuego, especially along the faults, are covered with saturated unconsolidated glacial deposits or peat.

Stability of monuments installed in these materials is a problem due to frost heaving and other surface processes. All sites, except the continuous station in Puerto Williams, were installed in rock outcrop to minimize problems due to monument stability. During the period 1998 to 2001, four measurement campaigns were performed in Argentina and most of the sites in Chile were remeasured once. Campaign measurement sites have therefore been occupied between two and four times over total observation spans of two to six years. The velocity field (Table 1, Figure 3), defined with respect to stable South America, clearly shows an increase in velocity from the north to the south with respect to stable South America. The velocity gradient is concentrated in the region of the Magallanes-Fagnano fault and is associated with the plate boundary. As expected, movement of the sites on the Scotia Plate side is almost directly east, which is left-lateral with respect to stable South America.

[11] The GPS data were processed using a distributed processing approach [*Feigl et al.*, 1993; *Oral*, 1994; *Zhang*, 1996; *Bock*, 1998] described by *Kendrick et al.* [1999, 2001]. GAMIT was used to process a regional data set composed of both continuous and campaign stations [*King and Bock*, 1998]. The continuous stations are processed every day, regardless of whether campaign stations are active. GLOBK was used to merge our daily regional solution with SOPAC's daily global solution in a free-network adjustment that takes full account of the covariance matrices [*Herring*, 1998; *Bock*, 1998]. By using a free-network solution, also known as an inner coordinate solution, the daily polyhedra formed by the GPS sites, rather than the individual site position time series, can be used as the basic data for velocity determination. Unless there is an earthquake or other effect generating an offset at some sites, the geometry of these polyhedra is essentially invariant from day to day, but evolves over months to years. To obtain site velocities, an iterative, weighted, regional linear alignment of the daily polyhedra is performed. This stacking stabilizes the site position time series (Figure 4), reducing the scatter of the time series and the error associated with the velocity estimation [*Kendrick et al.*, 1999, 2001].

[12] Error estimation, also described by *Kendrick et al.* [1999, 2001], follows the standard procedure of calculating the velocity covariance matrix assuming uncorrelated Gaussian errors with scaling by the post-fit scatter of the position time series [*Larson et al.*, 1997]. It is generally agreed that these estimates are optimistic due to the existence of colored or correlated noise in the GPS time series [*Larson et al.*, 1997; *Zhang et al.*, 1997, *Mao et al.*, 1999]. The error estimates, for both the continuous and campaign sites are therefore scaled based on the fractal gaussian noise model of *Zhang et al.* [1997]. Note that even with rescaling, the error estimates for the continuous stations are much smaller than those for the campaign stations. This is due to the larger number of observations for the continuous stations, over 1000, compared to the much smaller number of observations for the campaign stations, order 10, used to make the gaussian error estimate. *Santillan* [2003], using the processing method of *Kendrick et al.* [2001], examined the evolution of velocity estimates for continuous stations as a function of the time span used to determine them. Velocity estimates were updated monthly, each estimate having one month of additional data. For continuous stations in stable North America, the velocities stabilized after three to four years, with the new velocity estimations varying by less than the formal errors based on the unscaled Gaussian statistics. This suggests that at least some of the correlated errors are reduced using the network stacking procedure as compared to processing the position time series for each site independently.

[13] The free network (inner coordinate) solution is finally transformed into some useful outer coordinate or absolute reference frame, in this case a regional South American reference frame updated from *Kendrick et al.* [1999]. This step is not necessary to analyze the deformation associated with the plate boundary, but it is helpful for interpretation as it presents the velocities in a tectonically meaningful manner. For analysis of the

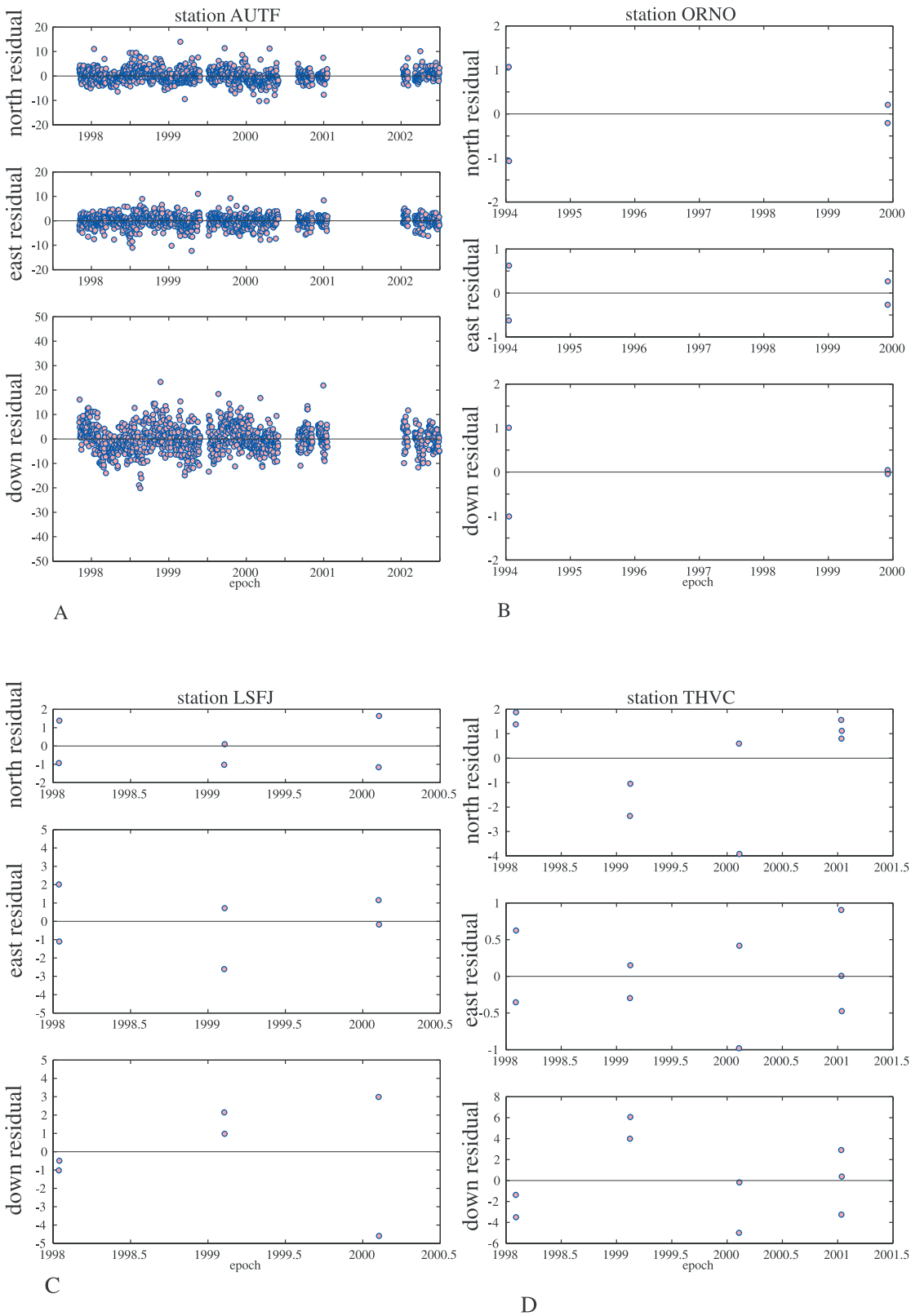

Figure 4. GPS position time series after removal of linear fit for velocity with respect to South America to show daily scatter for both continuous and campaign sites. (a) Continuous station AUTF, (b, c, d) campaign sites with 2, 3, and 4 occupations.

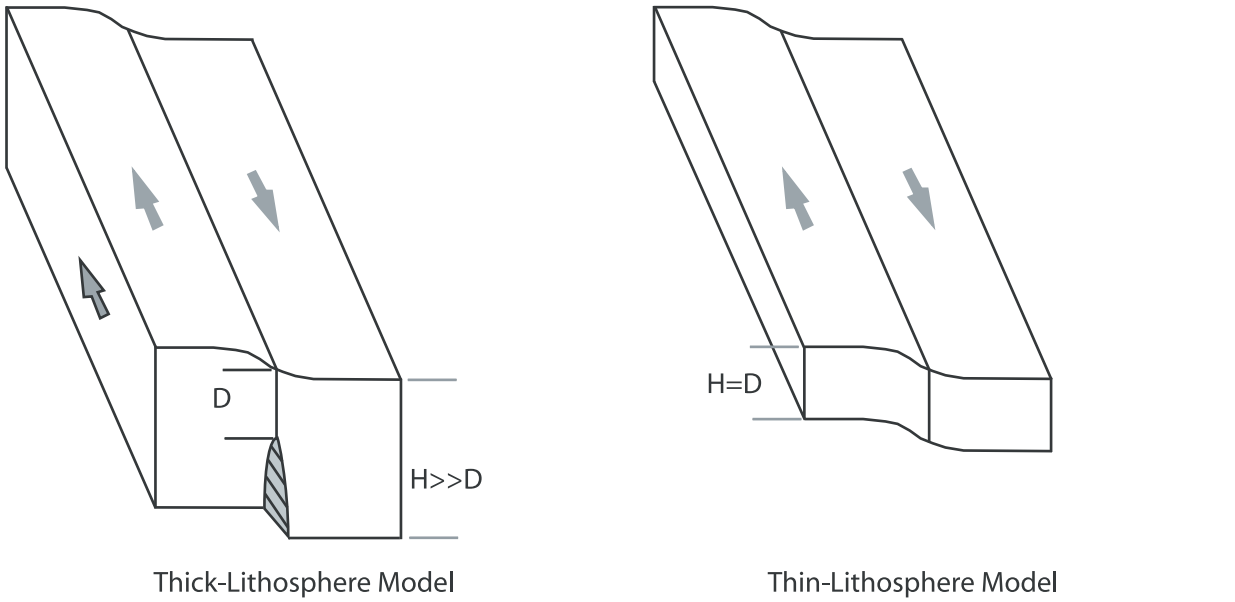

Figure 5a

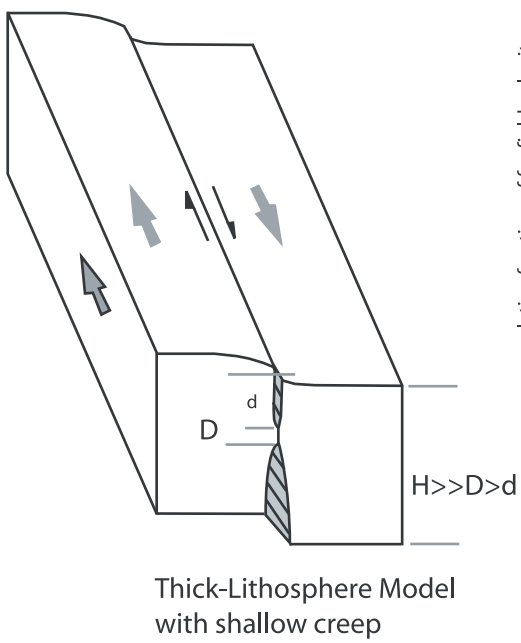

Figure 5b

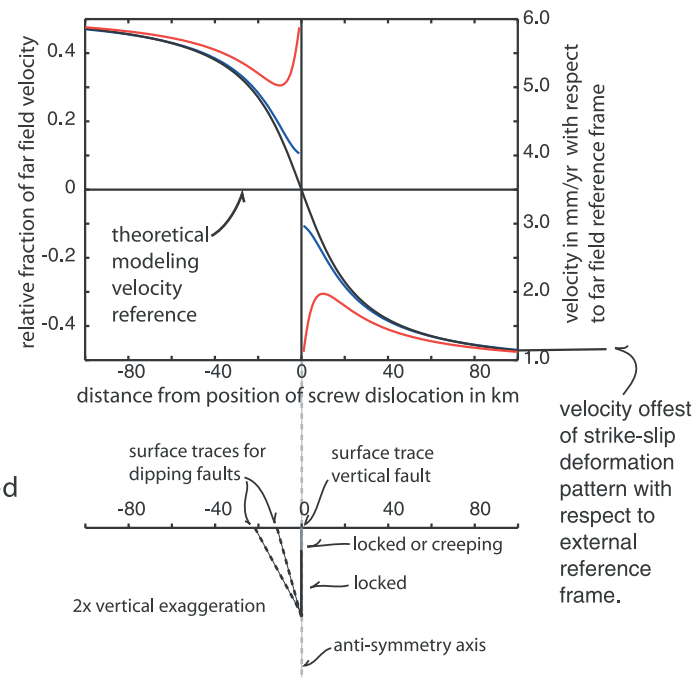

Figure 5c

deformation pattern across the plate boundary it is not necessary to propagate the errors in the reference frame definition because the free network processing correctly estimates the inner coordinate errors.

3. Modeling and Results

[14] There are two basic end-member models for strike-slip plate boundaries, the thick and thin lithosphere models (Figure 5a) [*Savage and Burford*, 1975]. Both are two-dimensional and consider the lithosphere to be a homogeneous elastic material. The thick-skinned model is a halfspace model with an embedded screw dislocation representing the fault. The screw dislocation defines the down-dip termination of the fault. Tectonically, the deformation across the fault is driven by equal and opposite far-field velocities. The thin-skinned model is a plate model, driven by basal forces. Both models predict the same surface deformation [*Thatcher*, 1983] (Figure 5c), so surface geodetic measurements cannot distinguish between them. *Savage and Burford* [1975] considered the thick lithosphere model, which is relatively straightforward to solve analytically [*Weertman and Weertman*, 1964] for both coseismic and interseismic deformation. The model has two parameters, locking depth and plate velocity, which can theoretically be determined by inversion of observed interseismic deformation. In the basic model the two parameters are completely decoupled and each controls an independent aspect of the model. The difference between the velocity asymptotes determines the relative plate velocity (Figure 5c). The shape of the deformation field is an inverse tangent that is a function of the dimensionless ratio x/D, where x is the distance from the fault and D is the depth of the screw dislocation or locking depth. The shape is therefore invariant and simply scales with the locking depth. The deformation field is limited to approximately 12 times the locking depth [*Lisowski et al.*, 1991] but the shape varies very little for geologically reasonable locking depths. This makes inversion for locking depth unstable [*Weertman*, 1965, 1973; *Parker*, 1977], as significant model variations may be statistically indistinguishable within the measurement errors. The locking depth, however, can be independently estimated from seismicity [*Brace and Byerlee*, 1970; *Sibson*, 1977, 1982, 1983; *Marone and Scholz*, 1988], and it is not uncommon to assume a geologically reasonable locking depth or use a seismically determined locking depth when inverting deformation data to estimate strike-slip fault parameters [e.g., *Murray and Segall*, 2001; *Miller et al.*, 2001]. Additional problems occur when there are multiple active faults that are less than several locking depths apart. This has the effect of coupling the depth and slip rate estimations because the asymptote information, which would otherwise independently control the slip rate estimation on an individual fault, is lost. In addition, the partitioning of the total motion between the faults also has to be estimated. In the San Francisco Bay Area, for example, estimates of slip rate on the

Figure 5. (opposite) (a) Thick and thin-lithosphere strike-slip fault models after *Savage and Burford* [1975]. Thick gray arrows without outlines are deep far-field or basal boundary conditions, thick gray arrows with black outline are far-field boundary conditions on the sides. The interseismic surface deformation field is continuous across fault. (b) Thick-lithosphere model with shallow creeping section. The interseismic surface deformation field is now discontinuous across fault, and is shown by solid arrows indicating slip at the surface. (c) The interseismic surface deformation or velocity for several models: thick skin model for a fault with a locking depth of 20 km (continuous black line) and for a fault locked from 5 to 20 km with shallow creep from 0 to 5 km depth for the superposition model (discontinuous red line, creep velocity same as far field velocity) and for the tectonically consistent model with a friction-free creeping section (discontinuous blue line). The blue and black lines bound the deformation pattern for the more realistic model that includes depth-dependent friction on the shallow creeping section [*Savage and Lisowski*, 1993]. The deformation field for the case of the creeping, friction-free fault was computed using the program 3-D DEF [*Gomberg and Ellis*, 1994]. The velocity scale on the left is in fraction of the plate rate with the velocity origin halfway between the two anti-symmetric far field asymptotes. The velocity scale on right is for a relative plate rate of 5 mm/yr with an offset of 1 mm/yr with respect to the reference frame. The reference frame is defined by additional measurements to the right where the velocities are zero. Cross section of model below the deformation pattern shows relationship between the position of the axis of the asymmetric deformation pattern and the positions of the down-dip end of the fault and the surface trace of the fault.

San Andreas fault depend on how the slip is partitioned between the various faults there. Estimation of slip on the San Andreas alone varies from 10.5 to 22.6 mm/yr while the locking depth estimates range from 4.7 to 44.6 km [*Freymueller et al.*, 1999; *Murray and Segall*, 2001].

[15] The model of a screw dislocation in an elastic halfspace can be easily extended to include shallow creeping behavior using the principle of linear superposition (Figures 5b and 5c). This allows estimation of the depth and velocity for the shallow creeping section. A problem with this approach is that the results for the creeping section are purely kinematic. As before, the velocity on the deeper section of the fault is interpreted to be the relative plate velocity and is directly related to the dynamics of the plate tectonic model. The properties of the creeping section, however, are found solely from a kinematic two-parameter fit for depth and slip velocity of the creeping section. A creeping fault should be driven by a combination of the plate motions plus the local stress concentration generated by the locked portion of the fault. The simplest version of this type of model has a shallow friction-free fault, which slips to relieve the local stress field produced by the locked section (Figures 5b and 5c). The surface deformation pattern is very different from that found by the superposition method in that it does not have the cusp near the fault. The displacement on the creeping part of the fault is also not uniform. It varies with depth as needed to balance the non-uniform driving forces applied to the unlocked shallow section of the fault. *Savage and Lisowski* [1993], following *Weertman* [1964], considered a more physically reasonable version of this model in which the fault includes a depth dependent frictional behavior. The deformation pattern for this model is bounded by that of the friction-free creep model and the basic single locked fault model. Owing to the difficulty of inverting the surface deformation data, estimates of the depth of the creeping section may depend on an alternate analysis that depends on the time rate of change of the stress and the creep rate across the fault rather than a fit to the deformation data [*Savage and Lisowski*, 1993]. The slip rate of the creeping section at the surface is directly measurable, by traditional or space geodetic techniques, due to offset across the fault.

[16] Deformation patterns associated with creeping faults are found both with and without the cusp shape [*Lyons et al.*, 2002]. Variation of the deformation from the two-dimensional behavior discussed above, such as the cusp, can be modeled by varying the depth of the locked or creeping sections along-strike [*Freymueller et al.*, 1999]. The analytic solutions discussed so far are two-dimensional and cannot model finite faults or faults whose properties vary along-strike. Numerical techniques, such as the elastic deformation code 3D-DEF [*Gomberg and Ellis*, 1994], can be used to model finite and non two-dimensional geometries and include faults that are driven by the stress field, rather than having displacement specified a-priori, although 3D-DEF does not include fault friction.

[17] To model the deformation associated with the Magallanes-Fagnano fault, a weighted least squares algorithm was used in a grid search inversion of the GPS velocities using the homogeneous elastic halfspace model of *Savage and Burford* [1975] discussed above. In addition to the two intrinsic parameters of the model, the strike and position of the anti-symmetric deformation pattern also have to be determined. In the theoretical discussion for interseismic deformation, the origin for distance is the point on the surface directly above the screw dislocation. This is the position of the axis of anti-symmetry of the surface deformation pattern. The ''fault position'' found in the inversion is therefore the surface position of the down-dip end of the fault, and not the position of the surface trace of the fault. For a vertical fault the surface trace of the fault is coincident with the origin. For a dipping fault the surface positions of the trace of the fault and the axis of anti-symmetry are not the same. The distance between them, together with the depth of the screw dislocation, provides an estimation of the dip. The origin for velocity in the theoretical discussion is half the relative plate velocity, since there is no absolute reference frame. In certain cases, however, choosing one side of the fault as the velocity reference, rather than the middle of the velocity range, allows one to estimate relative mo-

Table 2. Best-Fit Parameters, With Errors, for Model With an East-West Striking Fault Having a 15 km Locking Depth

	Position, Latitude	Velocity, mm/yr	Offset, mm/yr
−2σ	−54.66	5.27	0.64
Best fit	−54.54	6.60	1.40
+2σ	−54.43	7.91	2.23

tion between the strike-slip deformation pattern and the reference frame (Figure 5c). This could also be done by finding velocities for the two asymptotes, determining the relative velocity from their difference and estimating the velocity offset from their average. Applying this idea to the case of the San Andreas and western U.S. while using the eastern U.S. as the reference provides estimates for the Pacific-North America relative plate motion plus how this motion is partitioned between the narrow San Andreas transform boundary and the wider area of diffuse deformation of the Basin and Range. Applied to the Scotia-South America plate boundary, it allows estimation of partitioning of the South America-Scotia relative movement between the principal transform boundary plus tests for the existence of broader diffuse deformation. Such deformation could be associated with the proposed continued development of the Patagonian orocline or deformation associated with drag around the south-west corner of South America [*Diraison et al.*, 1997, 2000].

[18] Full inversion for the position, azimuth, locking depth, and velocity of an east-west striking fault is unstable due to the lack of suitable monument sites close to the fault and the limited along-strike aperture of the network. The across-strike sampling of the deformation field near the fault was limited by the scarcity of suitable monument sites due to the lack of rock outcrop and the geodetic instability of the surface geology. This prevented making a reliable estimate of the locking depth. Unfortunately,

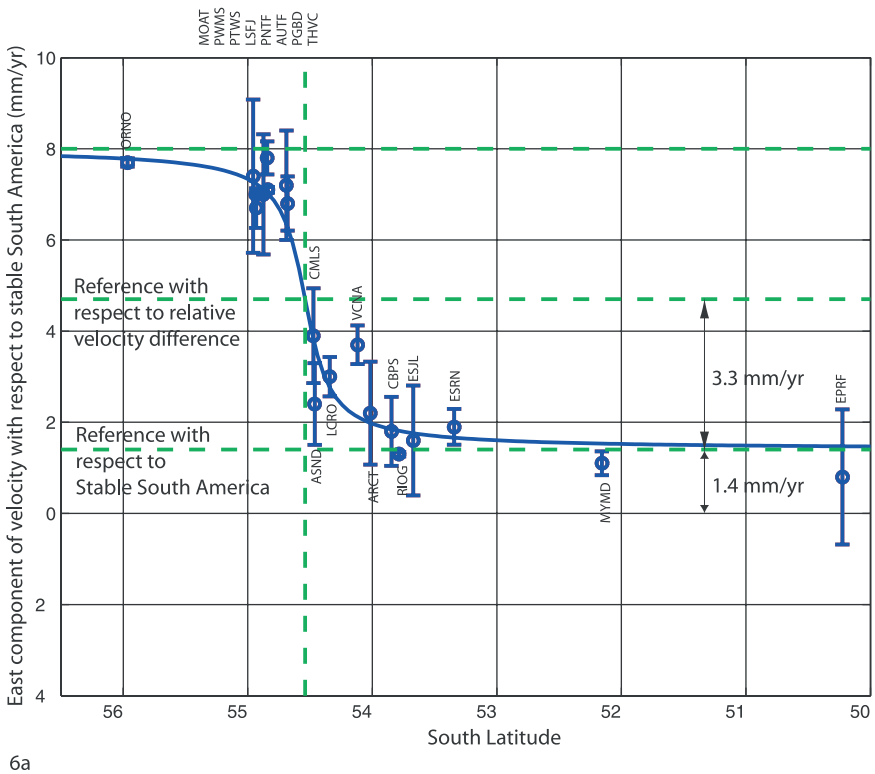

Figure 6. Fit of GPS data to simple strike-slip model of *Savage and Burford* [1975]. (a) Cross section of eastward component of velocity, v_e. Horizontal dashed green lines show velocity asymptotes and relative velocity axis. Vertical dashed green line shows horizontal location of the down-dip end of the fault or location of the screw dislocation. (b) Cross section of northward component of velocity, v_n, which shows no pattern.

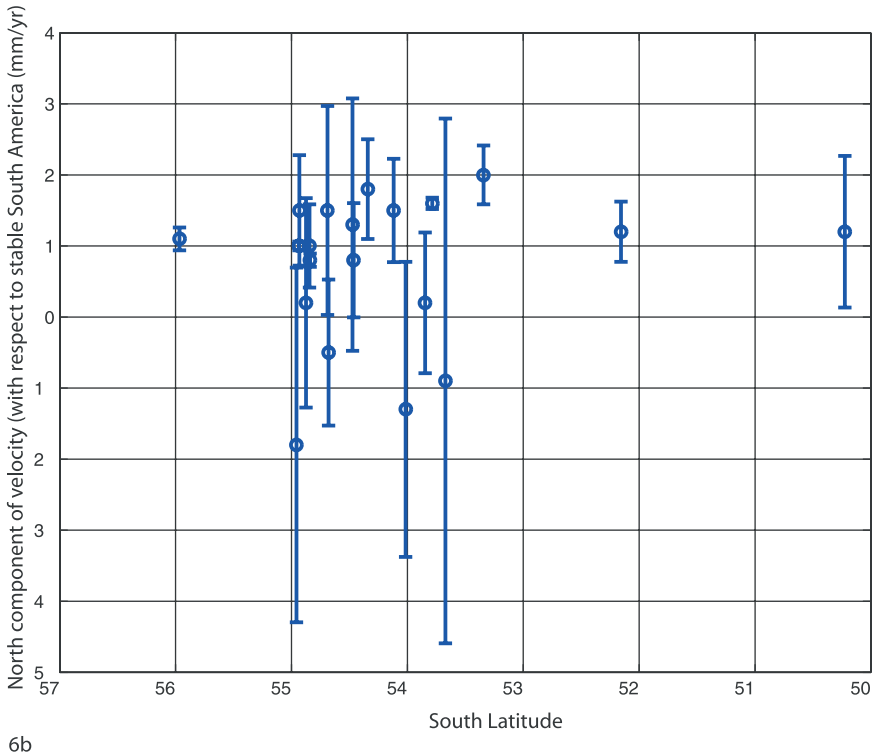

Figure 6. (continued)

the lack of seismic activity also precludes making an independent estimate of the locking depth. On the basis of the ability of the fault to generate mid to high magnitude 7 earthquakes, a depth of 15 km was assumed in the inversion for the remaining parameters. This is a reasonable estimate considering results for other strike-slip plate boundaries [*Murray and Segall*, 2001; *Thatcher*, 1990; *Beavan et al.*, 1999; *Leitner et al.*, 2001; *Wright et al.*, 2001]. The along-strike aperture of the network and three-dimensional geometric complications also prevent inverting for the strike of the model fault. The portion of the plate boundary in Tierra del Fuego is situated in a pure strike-slip section between a restraining bend to the west and a releasing bend to the east (Figure 1). The Magallanes-Fagnano fault through Lago Fagnano and the trace of the plate boundary at regional scale have east-west average strikes in the region of the network. The fault was therefore assumed to strike east-west, which is in general agreement with the velocity pattern.

[19] Results for the inversion for the fault parameters are given in Table 2 and shown in Figure 6a. For the grid search inversion, the N dimensional minimum of χ^2 estimates the parameter values in a least squares sense. The F-statistic [*Jenkins and Watts*, 1968] was used to determine the confidence intervals. The position of the down-dip end of the model fault is coincident with the surface trace of the Magallanes-Fagnano fault (latitude $-54.54° \pm 0.11°$) at the eastern end of Lago Fagnano, defining a vertical fault. Considering the uncertainty in location (±12 km) and the assumed depth of the down-dip end of the fault of 15 km, the estimated dip is $90° \pm 40°$. The relative velocity across this segment of the plate boundary was found to be 6.6 ± 1.3 mm/yr. Even though the sampling is sparse on the southern side of the Magallanes-Fagnano fault, the GPS velocities suggest that the major mapped faults there (Figure 2b) are not currently active.

[20] The model used to describe the deformation pattern is two-dimensional. The GPS network is concentrated in a north-south transect across Lago Fagnano, through which the fault is inferred to pass, but the exact trace of the fault in the lake is unknown. The mapped fault is not straight, con-

taining several en echelon offsets [*Cunningham*, 1993; *Klepeis*, 1994; *Diraison et al.*, 1997; *Lodolo et al.*, 2002]. Between Lago Fagnano and the Atlantic coast, east of most of the GPS network, the fault is relatively straight and strikes slightly south of east. It also includes a small lake that may be a small pull-apart structure in a releasing en echelon offset. To remain in Lago Fagnano, the fault has to bend, or contain en echelon offsets at a scale smaller than the lake. To the west, in Seno Almirantazgo, the strike of the fault bends approximately 30° to strike WNW-ESE and the fault continues to the triple junction in a relatively rectilinear manner with several restraining en echelon offsets (Figure 2a). In the area of the bend, there is also a sub-parallel fault, the Deseado fault, on the north side of the Magallanes-Fagnano fault. The average strike of Lago Fagnano is east-west, the direction chosen for the strike of the model fault. If the model fault is coincident with the trace of the Magallanes-Fagnano fault to the east of Lago Fagnano, it does not coincide with the fault in Lago Fagnano, or in Seno Almirantazgo to the west of the lake, without bends or en echelon offsets. Because the geometry of the GPS network is limited in both cross and along-strike sampling, it does not allow the GPS velocity field to resolve second-order deformations that may be caused by deviations of the fault from being straight, multiple fault strands, active transtension or transpression across en echelon offsets and small amplitude releasing or restraining bends. While geologically reasonable, it is not justifiable to use a more complicated fault model to fit the GPS data.

[21] Figure 6a shows that two sites on the north side of the fault, VCNA and ASND, on the north side of the fault are poorly modeled. A simple sensitivity analysis showed the results are highly sensitive to ASND, which is very close to the fault and therefore has a strong influence in defining the shape of the deformation field, but not VCNA, which is farther away and closer to the region of uniform asymptotic behavior. VCNA is one of several sites; that were measured only twice. The first measurement of these sites in 1994 used a tripod to position the antenna, a dual frequency C/A code receiver and a non-choke ring antenna. After 1995, all measurements were made using a fixed-height mast, a receiver with C/A tracking on L1 and Z-tracking on L2 and a choke ring antenna. The velocities for all the sites measured twice, except VCNA, are consistent with the tectonics and modeling. With only two measurements, it is difficult to evaluate the significance of velocity at VCNA. Additional measurements are necessary to establish if there may have been setup problems at VCNA, or if the velocity anomaly is real and a more complex model is needed to explain it. The site ASND, however, was measured four times over a period of three years, and the error is in the same range as that of the other sites. This suggests that the velocity there may be anomalous. ASND is just north of the eastern end of Lago Fagnano, which is located in a narrow, glacially carved valley that is at least 1 km deep along much of its length. The free sides of the valley can be thought of as the two sides of a creeping friction-free fault. The shape of Lago Fagnano in this area also suggests the possibility of this being the site of a releasing bend. This would accentuate conditions conducive to creep along this section of the fault by lowering the normal stress across the fault. Arguing for a locked fault, and against large-scale creep, however, is the fact that no geomorphologic evidence for creep along the subaerial part of the fault immediately east of Lago Fagnano has yet been observed and that this section of the fault ruptured in a large earthquake in 1949. The three-dimensional changes in the fault geometry here may be responsible for the deviation of the deformation field from that predicted by the simple two-dimensional halfspace model. A test of the inversion, which includes locking depth in addition to the relative velocity and velocity offset, was made with the two sites ASND and VNCA removed. This produced a result that is close to and statistically indistinguishable from the result of the inversion in which the depth was fixed at 15 km, while reducing the RMS by half.

[22] All the velocities are stated with respect to stable South America, so points distant from the plate boundary on the South American side should have zero, or due to uncertainty in the reference frame definition, small velocities. The velocity off-

set parameter allows the reference side of the fault to have a non-zero asymptotic velocity. This allows consideration of small motions of the sites used to define the fixed South America plate and/or allow for proposed regional deformations to occur across a wider boundary, such as that related to drag tectonics around the corner geometry of the triple junction [*Diraison et al.*, 1997]. This suggests consideration of a model similar to the western US where the relative plate motion is partitioned between the plate boundary and a region of distributed deformation in the continental plate [*Atwater*, 1970]. Considering the additional 1.4 ± 0.8 mm/yr of velocity offset between the strike-slip deformation pattern and stable South America, which is defined at the 1 mm/yr level, the GPS results suggest a velocity of 8.0 ± 2.1 mm/yr for the relative plate movements. This estimate is in agreement with the magnitudes of the velocities along the Beagle Channel and at Cape Horn (ORNO). The Euler pole of *Pelayo and Wiens* [1989] predicts 5.3 mm/yr left-lateral transtensional motion with respect to stable South America (Figure 3). The position of the pole was determined using slip vectors and transform azimuths, while the magnitude was determined by closure. The GPS vectors show a faster relative plate movement with a statistically insignificant transpressional component (Figure 6b).

[23] The north-south component of the velocity field (Figure 6b) is approximately constant across the network, averaging at about 1mm/yr to the north. Of the four sites that have a southerly component, three are based on measurements that span only two years. These estimations are not as reliable as those that span three years. The geology suggests extension in Southern Patagonia [*Diraison et al.*, 1997, 2000] and transtension along the Magallanes-Fagnano fault in Tierra del Fuego [*Lodolo et al.*, 2002], which would suggest an extensional component to the velocity field with respect to South America that should increase as the plate boundary faults are crossed while going south. Small regions of slow extensional tectonics are difficult to constrain with GPS as geologically significant structures can be produced by extension rates that are below the resolution of GPS. Block rotations, as suggested by *Diraison et al.* [1997], could explain areas with slightly northward movement relative to South America that would be consistent with rotating blocks. Rotations cannot explain, however, the relatively uniform northward motion across the whole network. The lack of any geological structures striking slightly north of east, parallel to the GPS vectors, argues against the model fault striking north of east. As the magnitude of the north-south component is within the uncertainties in the definition of the reference frame a strong interpretation of these results cannot make.

4. Conclusions

[24] The new GPS data allow a preliminary determination of several of the major properties of the segment of the Scotia-South America plate boundary that crosses Tierra del Fuego. In spite of the complexities of its geological history and current plate tectonic setting, the best model is a simple two-dimensional, vertical strike-slip fault, across which there is 6.6 ± 1.3 mm/yr relative plate motion. If the reports of 5 m offset for the 1949 event are accepted, which is reasonable for the magnitude of the event, the GPS rate of 6.6 mm/a results in a repeat time on the order of 750 years, although the uncertainty of this estimate is large. An additional 1–2 mm/year of relative plate motion may also be diffusely distributed across a large region in northern Tierra del Fuego and southernmost Patagonia. Such deformation is suggested by continued development of the south-western corner of South America as the unstable triple junction and the drag around the corner continue to evolve. The locking depth is poorly constrained by GPS, but considering the magnitude of the 1949 earthquake a locking depth of 15 km was assumed. The position for the downdip termination of the fault was coincident with the surface trace indicating a vertical fault. The error estimate in the position estimation gives an uncertainty of ±40° for the dip. Global plate models indicate ~22 mm/yr [*DeMets et al.*, 1990] left-lateral latitudinal motion of the South America plate with respect to the Antarctic plate. The implication has been that this is partitioned between transform faults along the North Scotia Ridge, the Shackleton Fracture Zone, and

the South Scotia Ridge (Figure 1). The velocity determined here for the motion across the boundary between the South America and Scotia plates appears to be compatible with motion of this order between the two major plates.

Acknowledgments

[25] The manuscript was greatly improved due to careful reviews by Mike Ellis at CERI, Associate Editor John Beavan, Chuck Demets and an anonymous reviewer. We would like to thank A. A. Garcia and F. Galbán of the Argentine Instituto Geográfico Militar (IGM), Lautaro Diaz, Hector Parra and Wilfredo Rubio of the Chilean IGM, M. S. Velasco of the Univ. Nac. de Buenos Aires and R. Knight of CERI for participation in the GPS fieldwork, the Argentine and Chilean IGMs, M. Caso and C. Coto and the staff of CADIC, Andrés Zakrajsek and H. Tassone of the Instituto Antártico Argentino, M. Plasencia, J. E. Cabrera, and N. J. Rossi of Univ. Nac. De La Plata, and G. Carreras, P. Rasso, A. R. Sánchez, F. H. Ferioli, G. A. Sánchez and G. M. Porro of Parques Nacionales de Argentina for operation of continuous stations. We would also like to thank the landowners in Tierra del Fuego and Patagoinia (Lawrence, Goodall, Paz, Henninger, Reyes, Viaña, Glubich, O'Bryne and Nieves families), Parques Nacionales de Argentina and TOTAL AUSTRAL for site access and their hospitality. This project was supported by NSF grants EAR-9116733 and OPP-9527925 (U Memphis), OPP-9530383 and EAR-9115576 (U Hawaii), OPP-9526687 (U Texas). This is CERI contribution 456, SOEST contribution 6145 and UTIG contribution 1650.

References

Adarnos, R. E., D. A. Weins, E. E. Vera, and P. J. Shore, Seismicity and tectonics of Patagonia from a local deployment of seismographs, *Eos Trans. AGU*, *80*, 726, 1999.

Atwater, T., Implications of plate tectonics for the Cenozoic tectonic evolution of western North America, *Geol. Soc. Am. Bull.*, *81*(12), 3513–3535, 1970.

Barker, P. F., I. W. D. Dalziel, and B. C. Storey, Tectonic development of the Scotia Arc region, in *The geology of Antarctica*, Monogr. on Geol. and Geophys., vol. 17, edited by R. J. Tingel, pp. 215–248, Oxford Univ. Press, New York, 1991.

Beavan, J., et al., Crustal deformation during 1994–1998 due to oblique continental collision in the central Southern Alps, New Zealand, and implications for seismic potential of the Alpine fault, *J. Geophys. Res.*, *104*, 25,233–25,255, 1999.

Bevis, M., Y. Bock, P. Fang, R. Reilinger, T. Herring, J. Stowell, and R. Smalley, Blending old and new approaches to regional geodesy, *Eos Trans. AGU*, *78*, 64–66, 1997.

Bock, Y., Medium distance GPS measurements, in *GPS For Geodesy*, edited by P. J. G. Teunissen and A. Kleusberg, 2nd ed., chap. 12, pp. 483–536, Springer-Verlag, New York, 1998.

Brace, W. F., and J. D. Byerlee, California earthquakes: Why only shallow focus?, *Science*, *168*, 1573–1576, 1970.

Bridges, T., Southern Mission: Tierra del Fuego, *South American Missionary Mag.*, *13*, 151–156, 1879.

British Antarctica Survey (BAS), Tectonic Map of the Scotia Arc, Misc. 3, British Antarctica Surv., Cambridge, 1985.

Bürgmann, R., E. Fielding, and J. Sukhatme, Slip along the Hayward fault, California, estimated from space-based synthetic aperture radar interferometry, *Geology*, *26*, 559–562, 1998.

Coffin, M. F., L. M. Gahagan, and L. A. Lawver, Present-day Plate Boundary Digital Data Compilation, *Tech. Rep. 174*, 5 pp., Univ. of Tex. Inst. for Geophys., Austin, 1998.

Cunningham, A. P., P. F. Barker, and J. S. Tomlinson, Tectonics and sedimentary environment of the north Scotia ridge region revealed by side-scan sonar, *J. Geol. Soc., London*, *155*, 941–956, 1998.

Cunningham, W. D., Strike-slip faults in the southernmost Andes and the development of the Patagonian Orocline, *Tectonics*, *12*, 169–186, 1993.

Cunninghan, W. D., K. A. Klepeis, W. A. Gose, and I. W. D. Dalziel, The Patagonian Orocline New paleomagnetic data from the Andean magmatic arc in Tierra del Fuego, Chile, *J. Geophys. Res.*, *96*, 16,061–16,067, 1991.

Cunningham, W. D., I. W. D. Dalziel, T.-Y. L. Lee, and L. A. Lawver, Southernmost South America-Antarctic Peninsula relative plate motions since 84 Ma: Implications for the tectonic evolution of the Scotia Arc region, *J. Geophys. Res.*, *100*, 8257–8266, 1995.

Dalziel, I. W. D., *Tectonics of the Scotia Arc*, Antarctica, 206 pp., AGU, Washington, D. C., 1989.

Dalziel, I. W. D., and R. L. Brown, Tectonic denudation of the Cordillera Darwin metamorphic core complex, Tierra del Fuego: Implications for cordilleran orogenesis, *Geology*, *17*, 699–703, 1989.

Dalziel, I. W. D., and D. H. Elliot, Evolution of the Scotia arc, *Nature*, *233*, 246–252, 1971.

Del Cogliano, D. R. Perdomo, and J.-L. Hormachea, Desplazamiento entre placas tectónicas en Tierra del Fuego, Actas de la XX Reunión Científica de la Asociación Argentina de Geología y Geofísica, Mendoza, 2000.

DeMets, C., R. G. Gordon, D. F. Argus, and S. Stein, Current plate motions, *Geophys. J. Int.*, *101*, 425–478, 1990.

DeWit, M. J., The evolution of the Scotia arc as a key to the reconstruction of southwestern Gondwanaland, *Tectonophysics*, *37*, 53–81, 1977.

Diraison, M., P. R. Cobbold, D. Gapais, and E. A. Rosello, Magellan Strait: Part of a Neogene rift system, *Geology*, *25*, 703–706, 1997.

Diraison, M., P. R. Cobbold, D. Gapais, E. A. Rosello, and C. Le Corre, Cenozoic crustal thickening, wrenching and rifting in the foothills of the southernmost Andes, *Tectonophysics*, *316*, 91–119, 2000.

Febrer, J. M., M. P. Plasencia, and N. C. Sabbione, Local and Regional Seismicity from Ushuaia Broadband Station Observations (Tierra del Fuego), *Terra Antartica*, *8*, 35–40, 2000.

Feigl, K., et al., Space geodetic measurements of crustal deformation in central and southern California, 1984–1992, *J. Geophys. Res.*, *89*, 21,677–21,712, 1993.

Forsythe, D. W., Fault Plane Solutions and Tectonics of the South Atlantic and Scotia Sea, *J. Geophys. Res.*, *80*, 1429–1443, 1975.

Freymueller, J. T., M. H. Murray, P. Segall, and D. Castillo, Kinematics of the Pacific-North American plate boundary zone, northern California, *J. Geophys. Res.*, *104*, 7419–7442, 1999.

Gomberg, J., and M. Ellis, Topography and tectonics of the central New Madrid seismic zone: Results of numerical experiments using a three-dimensional boundary-element program, *J. Geophys. Res.*, *99*, 20,299–20,310, 1994.

Herring, T., Documentation for GLOBK: Global Kalman filter VLBI and GPS analysis program, version 4.1, Mass. Inst. of Technol., Cambridge, 1998.

Jaschek, E., N. Sabbione, and P. Sierra, Reubicación de sismos localizados en territorio argentino (1920–1963), Observatorio Astronómico de la Universidad Nacional de La Plata, Serie Geofísica, N° 1, Tomo XI, 1982.

Jenkins, G. M., and D. G. Watts, Spectral Analysis and Its Applications, 138 pp., Holden-Day, San Francisco, Calif., 1968.

Kendrick, E. C., M. Bevis, R. Smalley, Jr., O. Cifuentes, and F. Galbán, Current rates of convergence across the Central Andes: Estimates from continuous GPS observations, *Geophys. Res. Lett.*, *26*, 541–544, 1999.

Kendrick, E. C., M. Bevis, R. Smalley, Jr., and B. Brooks, An integrated crustal velocity field for the central Andes, *Geochem. Geophys. Geosyst.*, *2*, doi:10.1029/2002GC000446, 2001.

King, R., and Y. Bock, Documentation for the GAMIT GPS analysis software, Release 9.7, Mass. Inst. of Technol., Cambridge, 1998.

Klepeis, K. A., The Magallanes and Deseado fault zones: Major segments of the South American-Scotia transform plate boundary in southernmost South America, Tierra del Fuego, *J. Geophys. Res.*, *99*, 22,001–22,014, 1994.

Kraemer, P. E., Palinspastic restoration of the Patagonian Orocline (50°S–56°S): A first attempt, XIV Congreso Geológico Argentino, Actas I, Salta, 241–244, 1999.

Larson, K., J. Freymueller, and S. Philipsen, Global plate velocities from the Global Positioning System, *J. Geophys. Res.*, *102*, 9961–9981, 1997.

Leitner, B., D. Egerhart-Phillips, H. Anderson, and J. L. Nablek, A focused look at the Alpine fault, New Zealand: Seismicity, focal mechanisms, and stress observations, *J. Geophys. Res.*, *106*, 2193–2220, 2001.

Lisowski, M., J. C. Savage, and W. H. Prescott, The velocity field along the San Andreas fault in central and southern California, *J. Geophys. Res.*, *96*, 8369–8389, 1991.

Lodolo, E., M. Menichetti, A. Tassone, R. Geletti, P. Sterazi, H. Lippai, and J. L. Hormachea, Researchers Target a Continental Transform Fault in Tierra del Fuego, *Eos Trans. AGU*, *83*, 1, 2002.

Lomnitz, C., Major Earthquakes and Tsunamis in Chile, *Geol. Rundschau*, *59*, 951, 1970.

Lyons, S. N., Y. Bock, and D. T. Sandwell, Near-field deformation of the Imperial Valley, Southern California, from GPS and InSAR measurements, in *Vistas for Geodesy in the New Millennium: Proceedings of the IAG 2001 Scientific Assembly, Budapest, Hungary*, edited by J. Adams and K. P. Schwarz, Springer-Verlag, New York, 2002.

Mao, A., C. G. A. Harrison, and T. H. Dixon, Noise in GPS coordinate time series, *J. Geophys. Res.*, *104*, 2797–2826, 1999.

Marone, C., and C. Scholz, The depth of seismic faulting and the upper transition from stable to unstable slip regimes, *Geophys. Res. Lett.*, *15*, 621–624, 1988.

Miller, M. M., D. J. Johnson, T. H. Dixon, and R. K. Dokka, Refined estimates of the Eastern California shear zone from GPS observations, 1993–1998, *J. Geophys. Res.*, *106*, 2245–2264, 2001.

Murray, M. H., and P. Segall, Modeling broadscale deformation in northern California and Nevada from plate motions and elastic strain accumulation, *Geophys. Res. Lett.*, *28*, 4315–4318, 2001.

Olivero, E. B., and N. Malumián, Eocene Stratigraphy of Southeastern Tierra del Fuego Island, Argentina, *AAPG Bull.*, *83*(2), 295–313, 1999.

Olivero, E. B., and D. R. Martinioni, A review of the geology of the Argentinian Fuegian Andes, *J. Soc. Am. Earth Sci.*, *14*, 175–188, 2001.

Olivero, E., E. Malagnino, and D. Gaglliardini, Interpretación preliminar del sistema de fracturas del este de Tierra del Fuego basada en imagines ERS-1: SELLPER, Revista Técnica de Integración Iberoamericana y Mundial, 11, pp. 34–39, 1995.

Oral, M. B., Global Positioning System (GPS) measurements in Turkey (1988–1992): Kinematics of the Africa-Arabia-Eurasia plate collision zone, Ph.D. thesis, Mass. Inst. Technol., Cambridge, 1994.

Parker, R. L., Understanding inverse theory, *Annu. Rev. Earth Planet. Sci.*, *5*, 35–64, 1977.

Pelayo, A. M., and D. A. Wiens, Seismotectonics and relative plate motions in the Scotia region, *J. Geophys. Res.*, *94*, 7293–7320, 1989.

Santillan, V. M., Deformation in the New Madrid Seismic Zone from continuous GPS geodesy, M. S. thesis, Univ. of Memphis, Memphis, Tenn., 2003.

Savage, J. C., and R. O. Burford, Geodetic Determination of relative plate motion in central California, *J. Geophys. Res.*, *78*, 5832–7845, 1975.

Savage, J. C., and M. Lisowski, Inferred depth of creep on the Hayward fault, central California, *J. Geophys. Res.*, *98*, 787–793, 1993.

Schwartz, D. P., H. D. Stenner, C. Costa, R. Smalley, M. Ellis, and M. S. Velasco, Paleoseismology at the End of the World: Initial observations of the Fagnano fault, Tierra del Fuego, Argentina, *Seismol. Res. Lett.*, *72*, 265, 2001.

Sibson, R. H., Fault rocks and fault mechanisms, *J. Geol. Soc., London*, *133*, 191–213, 1977.

Sibson, R. H., Fault zone models, heat flow, and the depth distribution of earthquakes in the continental crust of the

United States, *Bull. Seismol. Soc. Am.*, *72*, 151–163, 1982.

Sibson, R. H., Continental fault structure and the shallow earthquake source, *J. Geol. Soc. London*, *140*, 741–767, 1983.

Thatcher, W., Nonlinear strain buildup and the earthquake cycle on the San Andreas fault, *J. Geophys. Res.*, *88*, 5893–5902, 1983.

Thatcher, W., Present-day crustal movements and the mechanics of cyclic deformation, 189–205, in The San Andreas fault system, California, *U.S. Geol. Soc. Prof. Pap.*, *1515*, 1990.

Weertman, J., Continuum distribution of dislocations on faults with finite friction, *Bull. Seismol. Soc. Am.*, *54*(4), 1035–1058, 1964.

Weertman, J., Relationship between displacements on a free surface and the stress on a fault, *Bull. Seismol. Soc. Am.*, *55*, 945–953, 1965.

Weertman, J., A reply, *Bull. Seismol. Soc. Am.*, *63*, 2191–2192, 1973.

Weertman, J., and J. R. Weertman, *Elementary Dislocation Theory*, 213 pp., Macmillan, New York, 1964.

Winslow, M. A., Mechanisms for basement shortening in the Andean foreland fold belt of southern South America, in *Thrust and Nappe Tectonics*, edited by K. R. McClay and N. J. Price, *Spec. Publ. Geol. Soc. London*, *9*, 275–292, 1981.

Wright, T., B. Parsons, and E. Fielding, Measurement of interseismic strain accumulation across the North Anatolian Fault by satellite radar interferometry, *Geophys. Res. Lett.*, *28*, 2117–2120, 2001.

Zhang, J., Continuous GPS measurements of crustal deformation in southern California, Ph.D. dissertation, Univ. of Calif., San Diego, 1996.

Zhang, J., Y. Bock, H. Johnson, P. Fang, S. Williams, J. Genrich, S. Wdowinski, and J. Behr, Southern California Permanent GPS Geodetic Array: Error analysis of daily position estimates and site velocities, *J. Geophys. Res.*, *102*, 18,035–18,055, 1997.